Electrochimica Acta 191 (2016) 284–298

Contents lists available at ScienceDirect

Electrochimica Acta

journal homepage: www.elsevier.com/locate/electacta

Performance evaluation of conductive additives for activated carbon supercapacitors in organic electrolyte

N. Jäckel[a,b,1], D. Weingarth[a], A. Schreiber[a], B. Krüner[a,b], M. Zeiger[a,b], A. Tolosa[a,b], M. Aslan[a], V. Presser[a,b,*]

[a] INM—Leibniz Institute for New Materials, Campus D2 2, 66123 Saarbrücken, Germany
[b] Department of Materials Science and Engineering, Saarland University, Campus D2 2, 66123 Saarbrücken, Germany

ARTICLE INFO

Article history:
Received 2 July 2015
Received in revised form 21 November 2015
Accepted 10 January 2016
Available online 16 January 2016

Keywords:
supercapacitor
conductive additive
activated carbon
rate capability
performance evaluation
long-time stability

ABSTRACT

In this study, we investigate two different activated carbons and four conductive additive materials, all produced in industrial scale from commercial suppliers. The two activated carbons differed in porosity: one with a narrow microporous pore size distribution, the other showed a broader micro-mesoporous pore structure. Electrochemical benchmarking was done in one molar tetraethylammonium tetrafluoroborate in acetonitrile. Comprehensive structural, chemical, and electrical characterization was carried out by varied techniques. This way, we correlate the electrochemical performance with composite electrode properties, such as surface area, pore volume, electrical conductivity, and mass loading for different admixtures of conductive additives to activated carbon. The electrochemical rate handling (from 0.1 A g^{-1} to 10 A g^{-1}) and long-time stability testing via voltage floating (100 h at 2.7 V cell voltage) show the influence of functional surface groups on carbon materials and the role of percolation of additive particles.

1. Introduction

Electrical double-layer capacitors (EDLCs, also known as supercapacitors or ultracapacitors) are energy storage devices with high efficiency and long lifetime durability [1–3]. Today, EDLCs are used in electric vehicles, energy recuperation modules, systems for uninterrupted power supply, or fast recharging energy modules for high-power applications [4]. In EDLCs, energy storage is accomplished via ion electrosorption in the electrical double-layer (EDL) at the electrically charged interface of high surface area carbon electrodes with an electrolyte, being typically aqueous or organic solvent based [5]. Supercapacitors excel in high power handling and longevity, but they show only a moderate energy density compared to lithium-ion batteries [6,7]. The electrochemical performance of supercapacitors is related to the pore structure and high values are obtained for high surface area materials, such as activated carbon (AC) [3,8,9]. In particular, carbons for supercapacitor application must show a well-developed porosity and pore size distribution, which have to be optimized for a certain electrolyte system with matching the ion size and pore size [10–14].

Supercapacitor electrodes require mechanical binding of carbon particles [9,15]. This is commonly accomplished by using polymeric binders. Dependent on the polymer, typically 5-15 mass % are needed to obtain film electrodes with sufficient mechanical integrity [4]. To overcome the intrinsically low electrical conductivity of such film electrodes, conductive additives like carbon black (CB) with a specific surface area (SSA) of typically below 100 $m^2 g^{-1}$ and average primary particle sizes of about or less than 50 nm are added [16,17]. There are also carbon additives with a high surface area, for example, some CBs show a SSA of ca. 1500 $m^2 g^{-1}$ while preserving a nanoscopic size of below 50 nm [4]. In addition to CB, also other materials have been explored as conductive additive, such as carbon nanotubes, graphite nanoparticles, or carbon onions [16–22]. Typically, the literature reports an optimum amount of conductive additive at around 5 mass% [16,19,20]. When we consider that most carbon powders with a high intrinsic electrical conductivity, especially those used as conductive additives, have a much smaller SSA compared to typical AC, we see that mixing results in a lower total surface area of the electrode and a lower equilibrium capacitance [18]. However, to enhance the power handling ability, admixing of conductive additives still is a very practical approach.

* Corresponding author.
E-mail address: volker.presser@leibniz-inm.de (V. Presser).
[1] ISE member.

http://dx.doi.org/10.1016/j.electacta.2016.01.065
0013-4686/

As shown previously, the admixture of conductive additives to an AC particle matrix does not always improve the electrochemical performance [18]. Especially at a low specific current, the decrease in total SSA by adding a low surface material to AC leads to a drop in gravimetric capacitance. Nevertheless, the electrical conductivity can be increased with an improved capacitance retention at high loads. Especially small additive particles with low tendency of forming aggregates are preferred because of the facile dispersibility and resulting distribution homogeneity within a composite electrode (i.e. lowering the percolation threshold) [17]. The optimal amount of conductive additive also depends on the target application and the electrolyte system. For example, in 1 M TEA-BF_4/ACN (TEA-BF_4 = tetraethylammonium tetrafluoroborate; ACN = acetonitrile), the optimum amount of additive was found to be 5 mass%, whereas in 1 M TEA-BF_4/PC (PC = propylene carbonate) the best performance was reached at 2.5 mass% admixture of conductive additives like high and low SSA carbon black and carbon onions [18].

Developing an improved supercapacitor with high power handling cannot be accomplished without addressing device lifespan. Typically, supercapacitors are assume to last over hundreds of thousands of charge and discharge cycles [2]. The actual lifespan strongly depends on the operation mode and temperature [13,23]. Device lifetime also concerns the selection of a suitable cell voltage window in which stable performance is possible [24]. Even when only operating within the electrochemical stability window, carbon electrodes will age over time [23]. In particular, the performance stability is challenged by electrochemical degradation of surface functional groups on the carbon surface, which can react with the electrolyte and decomposition products may cause pore blocking [25]. A suitable way of accelerated aging testing is voltage floating, which is in case of EDLC more adequate to reveal limitations to the cell operation compared to voltage cycling [23]. During floating testing, gas evolution can take place resulting from the decomposition of the electrolyte [24,26]. Compared to many AC materials, higher ordered materials such as CB tend to have a lower concentration of surface groups and a

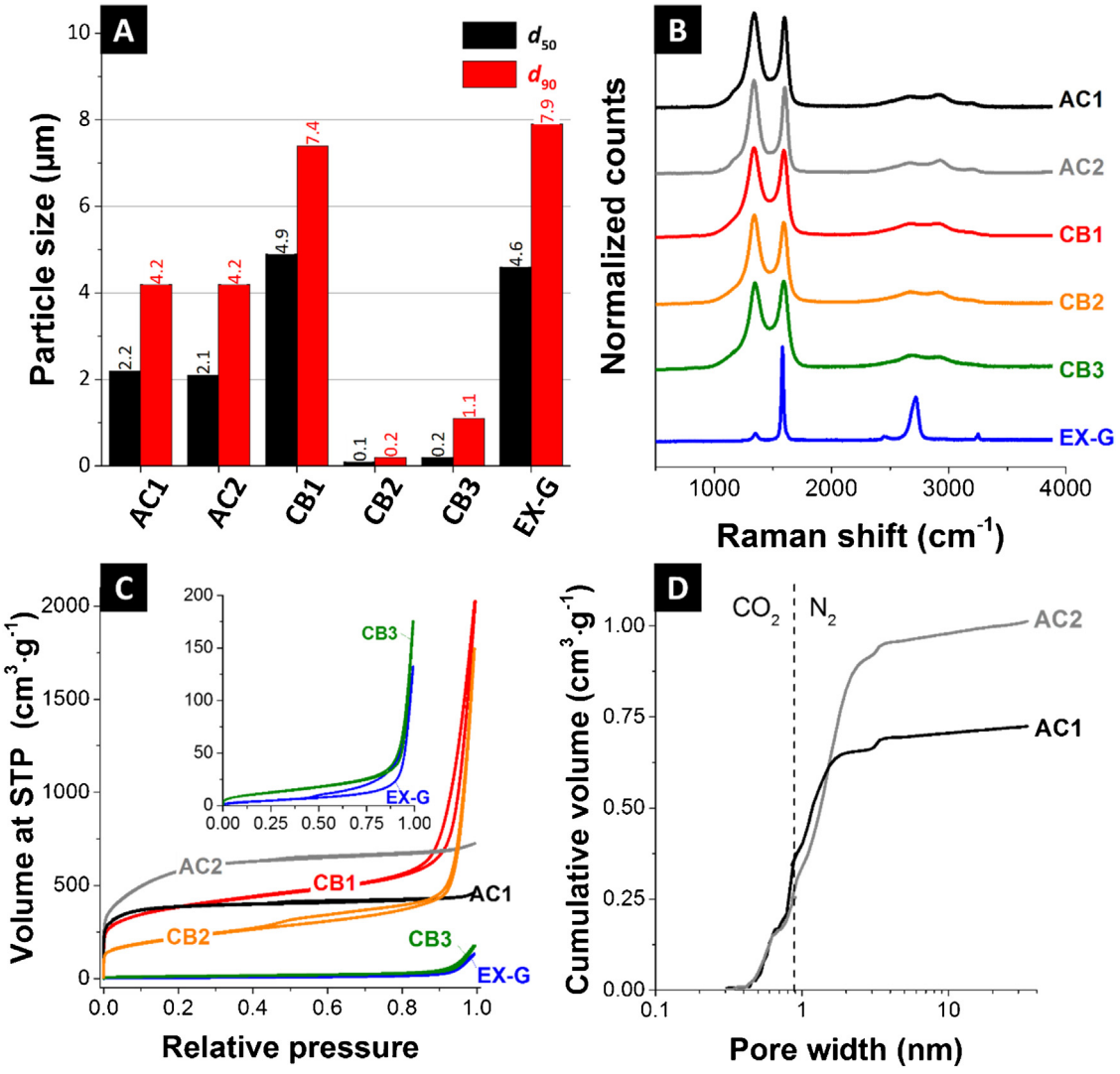

Fig. 1. (A) Particle size distribution of the used carbon materials, derived by centrifugal sedimentation analyses. (B) Raman pattern with increasing degree of ordering from upper to lower pattern. (C) Nitrogen sorption isotherms of the materials without binder (inset: zoom on CB3 and EX-G only; the inset has the same units on the axes as the main graph). (D) Pore volume distribution of the two activated carbons. Below 1 nm, the data is derived by carbon dioxide sorption measurements and above 1 nm from nitrogen sorption data.

higher affinity to yield better long-term stability [23,25]. Yet, the role of surface functionalities on the performance stability in composite film electrodes (i.e., AC plus conductive additive plus polymer binder) remains poorly understood.

This study provides a comprehensive comparison of four different conductive additives used for two kinds of activated carbon electrodes. Electrodes with up to 10 mass% of conductive additive were investigated by structural measurements like transmission electron microscopy (TEM), elemental analysis (EDX), streaming potential, and gas sorption analysis. The electrochemical performance was measured via rate capability in galvanostatic mode. Long-time stability tests were carried out over 100 h of voltage floating at 2.7 V.

2. Experimental description

2.1. Electrode materials and preparation

Two commercial steam-activated coconut-derived activated carbon powders (AC) were used, namely type YP-50F and YP-80F (Kuraray Chemicals Co., Japan), called AC1 and AC2, respectively. Different commercial conductive additives were used: high surface area carbon black BP2000 (Cabot, USA; called CB1), medium SSA carbon black Ensaco350 (CB2) and low surface area carbon black Super C65 (CB3). The latter two were provided by Imerys Graphite & Carbon, Switzerland. Another additive was an experimental expanded graphite (EX-G). The conductive additives were added to AC at an amount of 2.5 mass%, 5 mass%, and 10 mass% ("100%" with respect to the total carbon mass without binder).

For electrode preparation, a uniform distribution of AC and additive components was obtained by mixing the materials as an ethanolic slurry. For this, 1 g of carbon powder (i.e., activated carbon plus conductive additive) was dispersed in 20 mL ethanol. The slurry was sonicated for 15 min and then heated to 90 °C while stirring to evaporate the ethanol until the slurry became paste-like consistency. 5 mass% of dissolved polytetrafluoroethylene (PTFE, 60 mass% solution in water from Sigma Aldrich, USA) were added as binder (for electrodes only composed of conductive additive materials: 10 mass% PTFE). The resulting material was rolled with a rolling machine (MTI HR01, MTI Corp., USA) to a 200 ± 20 μm thick free standing film electrode and finally dried at 120 °C at 2 kPa for 24 h before use.

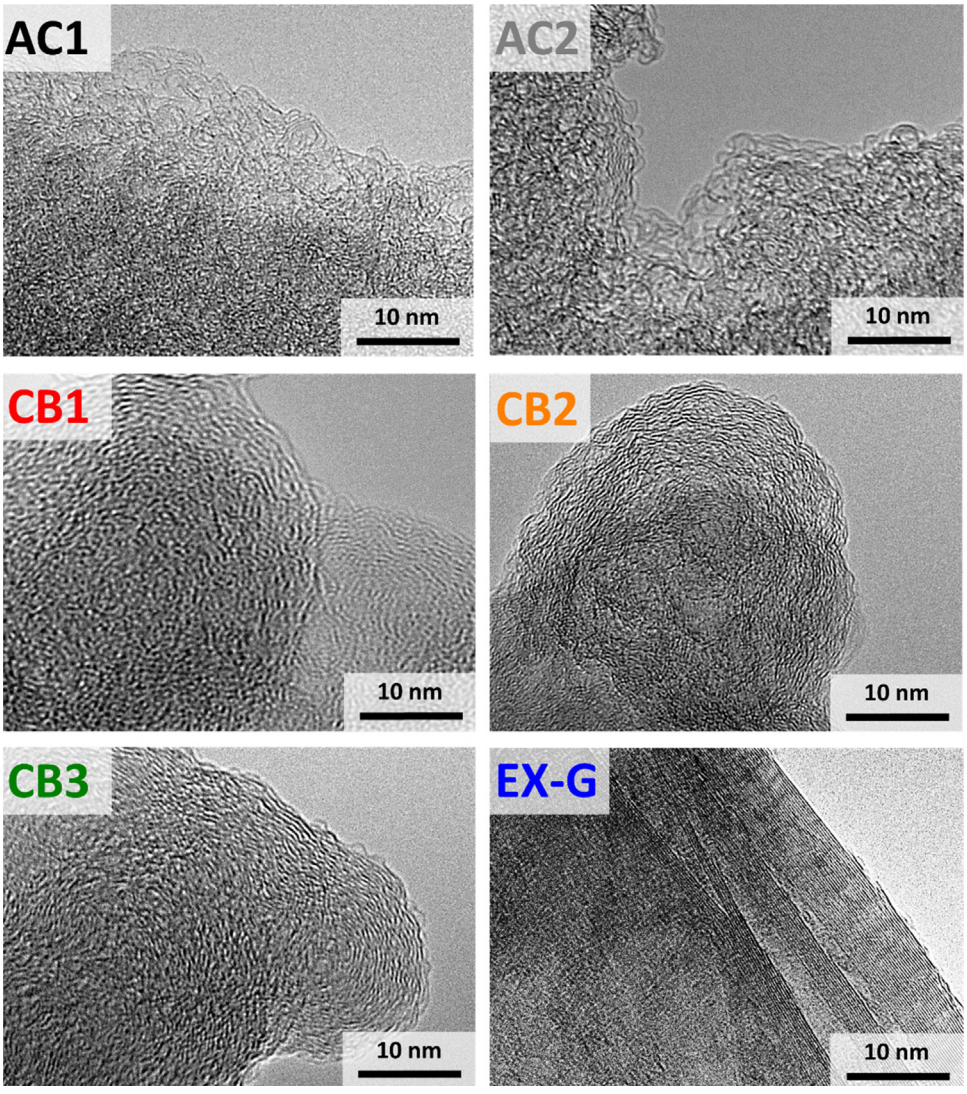

Fig. 2. TEM micrographs of the materials used in this study.

2.2. Cell preparation, electrical, and electrochemical measurements

Sheet resistance measurements were made with a custom-built spring-loaded four-point probe with blunt gold contacts (tip diameter: 1.5 mm, tip distance: 3 mm). For electrochemical testing, we employed a custom-built polyether ether ketone (PEEK) cell with spring loaded titanium pistons as a three electrode system described elsewhere [27]. Electrode discs (same mass and material for the working- and counter electrode) with 12 mm diameter and 200 ± 20 μm thickness were punched out of the free standing film electrode (total mass of carbon in a symmetrical cell was 20 ± 5 mg) and separated by a glass-fiber separator (GF/A from Whatman, USA) and placed on a carbon-coated aluminum foil current collector (type Zflo 2653 from Coveris Advanced Coatings, USA) [28,29]. The assembled cells were dried at 120 °C for 12 h at 2 kPa in an inert gas glove box (MBraun Labmaster 130, O_2 and $H_2O < 1$ ppm) and, after cooling to room temperature, vacuum-filled with 1 M tetraethylammonium tetrafluoroborate (TEA-BF_4) in electrochemical grade acetonitrile (ACN) purchased from BASF, Germany (i.e., water content <20 ppm).

Electrochemical measurements were carried out using a potentiostat/galvanostat VSP300 from Bio-Logic, France, with cyclic voltammetry (CV) and galvanostatic cycling with potential limitation (GCPL). CVs were recorded in full cell mode at 10 mV s^{-1} in the potential range from 0-2.5 V cell voltage. In GCPL mode, the specific current was increased in several steps from 0.1 A g^{-1} to 10 A g^{-1} with 10 s resting period between charging/discharging to access information on the IR-drop.

The gravimetric capacitance during discharging was calculated via Eq. (1):

$$C_{sp} = 4 \cdot \frac{\left(\int_{t_0}^{t_{end}} Idt\right)}{U} \cdot \frac{1}{m} \quad (1)$$

with specific capacitance C_{sp}, time t (t_0: starting time of discharge, t_{end}: end of discharging time), IR-drop corrected cell voltage U, and total mass of the electrodes m (i.e., considering carbon and the binder). For every type of electrode composition, four electrodes were prepared and these two cells were tested individually to calculate mean values. Long-time stability tests were made after rate capability test in galvanostatic mode at 2.7 V cell voltage for 100 h with measuring capacitive retention every 10 h at 1 A g^{-1} with cell potential 0-2.5 V.

2.3. Porosity analysis

Nitrogen gas sorption measurements were carried out with an Autosorb iQ system (Quantachrome, USA) at the temperature of liquid nitrogen (-196 °C) after outgasing (at 150 °C for 10 h for electrode samples and at 300 °C for 24 h for powder samples) at about 10^2 Pa. The relative pressure range was varied from $5\,10^{-7}$ to 1.0 in 68 steps. The specific surface area (SSA) was calculated with the ASiQwin-software using the Brunauer–Emmett–Teller (BET) equation [30] in the linear relative pressure range 0.01-0.2. We also calculated the SSA and pore size distribution (PSD) via quenched-solid density functional theory (QSDFT) with a slit model and pore size between 0.56 and 37.5 nm [31]. Values for the total pore volume correspond to $p/p_0 = 0.95$. Carbon dioxide gas sorption measurements were carried out at 0 °C in the relative pressure range from $1{\cdot}10^{-4}$ to $1{\cdot}10^{-2}$ in 40 steps. SSA and PSD values were calculated for pore sizes between 0.3 and 1 nm with the ASiQwin software using nonlocal density functional theory (NLDFT) for CO_2 sorption [32,33].

2.4. Effective density and particle size distribution analysis

The particle size distribution of carbon powders was measured using centrifugal sedimentation analysis (LUMiSizer from LUM GmbH, Germany). In a typical measurement, the powder was dispersed in ethanol (0.25 mg mL^{-1}), sonicated for 30 min, and measured at 200-4000 rpm. A dispersion in ethanol was chosen for comparability with the situation during actual electrode preparation (which involved ethanolic suspensions). The starting transmission for all samples was 25-60%. The d_{90} and d_{50} values denote the particle size in the cumulative particle size distribution encompassing 90 vol% and 50 vol%, respectively.

For measurements of the effective electrode density, an as-prepared 5×5 cm^2 sized film electrode was post-compacted with 1 kN cm^{-2} to ensure a constant compaction level and analyzed gravimetrically. The thickness after compaction was measured at four points with a micrometer caliper (Digi-Met from Helios-Preisser, Germany).

2.5. Structural characterization

Samples for transmission electron microscopy (TEM) were dispersed and sonicated in ethanol and placed on a copper grid with a thin lacey carbon film (Gatan Inc., USA). TEM images were recorded with a JEOL 2100F system at 200 kV in vacuum. EDX spectra of carbon powders were measured with a Thermo Fisher Scientific system placed in a JSM-7500F from JEOL, Japan. Carbon powder samples were placed on a conductive carbon tape and spectra were recorded at 50 different positions for each sample with 10 kV acceleration voltage. The composition of the composite electrodes was measured by energy dispersive X-ray spectroscopy (EDX) mapping using a X-Max-150 detector from Oxford Instruments attached to the SEM chamber. Using an accelerating voltage of 5 kV and an emission current of 10 μA, the mapping was measured and the average of 3 values were calculated. The aged (positive) electrodes were several times washed in neat acetonitrile to remove the salt from the electrolyte inside the glovebox. Afterwards they were dried in vacuum and put into the SEM chamber.

Raman spectra of the raw materials were recorded with a Renishaw inVia Raman system using an Nd-YAG laser (532 nm) with 0.2 mW power at the sample's surface. The spectral resolution of ca. 1.2 cm^{-1} corresponds to a grating with 2400 lines mm^{-1} and

Table 1
Raman data fitted with two Lorentzian peaks, one for the D-band and one for the G-band.

Material	D-mode position (cm^{-1})	G-mode position (cm^{-1})	FWHM D-mode (cm^{-1})	FWHM G-mode (cm^{-1})	Integral I_D/I_G ratio
AC1	1338	1596	140	65	2.2
AC2	1337	1599	161	76	2.1
CB1	1339	1589	212	100	2.1
CB2	1341	1589	145	78	2.0
CB3	1350	1588	173	89	1.8
EX-G	1350	1581	20	45	0.1

Table 2
Specific surface area of used powder materials. BET-SSA and QSDFT-SSA, pore volume and average pore size.

Material	BET SSA ($m^2 g^{-1}$)	QSDFT SSA ($m^2 g^{-1}$)	Pore volume ($cm^3 g^{-1}$)	Average pore size (nm)
AC1	1681	1560	0.78	0.9
AC2	2347	1756	1.15	1.6
CB1	1389	1272	1.92	19
CB2	770	715	0.77	14
CB3	65	56	0.15	27
EX-G	20	21	0.10	46

Table 3
Chemical analysis via EDX shows the different amount of carbon and oxygen in powder samples.

Material	Carbon (atom%)	Oxygen (atom%)
AC1	97.4 ± 0.5	2.4 ± 0.5
AC2	97.8 ± 0.5	2.0 ± 0.5
CB1	98.1 ± 0.1	1.3 ± 0.1
CB2	97.9 ± 0.1	1.9 ± 0.1
CB3	98.9 ± 0.1	0.9 ± 0.1
EX-G	98.8 ± 0.6	1.0 ± 0.5

the spot size on the sample was in the focal plane ca. 2 μm (numeric aperture = 0.9). The acquisition time was 30 s and 50 accumulations were recorded. Peak analysis and peak fitting were performed assuming one Lorentzian peak for each the D-mode and the G-mode.

Streaming potential measurements were made in a Mütek PCD (BTG Eclépens, Switzerland) with 100 mg carbon powder dissolved in 30 mL DI water. Suspensions were first sonicated for 10 min, followed by a homogenization step of 48 h on a moving table. Prior to the experiment, the starting pH value was set to 9.5 with aqueous 50 mM NaOH solution, which was corrected after another 10 h homogenization on a moving table. For each measurement 20 mL suspension was titrated to an end pH value of 3 by using 50 mM HCl.

3. Results and discussion

3.1. Structure, porosity, and chemistry of the powder materials

Particle size analysis of the carbon materials is a first important characterization method. We chose two common commercial-grade steam-activated coconut-derived carbons with anisomeric shape [18] and typical agglomerate size of several micrometers ($d_{50} \approx 2$ μm, $d_{90} \approx 4$ μm; Fig. 1). This is a typical value for AC materials used for supercapacitor electrodes [34]. The high SSA carbon black CB1 showed aggregates and particle clusters in the range of 1-10 μm ($d_{50} = 4.9$ μm, $d_{90} = 7.4$ μm), whereas these values are in contrast to the much smaller primary particle size in the range of 20-50 nm seen in the TEM images (Fig. 2). CB2 shows no cluster formation ($d_{50} = 0.1$ μm, $d_{90} = 0.2$ μm) and CB3 forms much smaller clusters below 1 μm ($d_{50} = 0.2$ μm, $d_{90} = 1.1$ μm) even if the primary particle size is about 100 nm, according to TEM (Fig. 2). The flake size of EX-G is in the micrometer range ($d_{50} = 4.6$ μm, $d_{90} = 7.9$ μm).

The materials also differ in the degree of carbon ordering, as evident from Raman analysis (Fig. 1B) and TEM micrographs (Fig. 2). Raman spectra are characterized by the D-mode between 1337 and 1350 cm^{-1} and the G-mode between 1581 and 1599 cm^{-1}. The G-mode is related to the bond stretching of sp^2-hybridized carbon atoms in rings and chains according to the zone center E_{2g} mode [35]. The double-resonant D-mode, or "disordered" mode, arises due to the breathing of six-fold rings, but is only Raman active in the presence of defects, such as related to curvature, edges, heteroatoms, or vacancies [36]. The graphite flakes (EX-G) demonstrate the Raman spectrum of nearly ideal graphite with a G-mode at 1581 cm^{-1}, sharp peaks, and a very small D-mode, resulting in an integral intensity ratio I_D/I_G of 0.1 (Table 1). The G-mode position varies between 1588 and 1589 cm^{-1} for the different carbon blacks used in this study (CB1-CB3). Compared to ideal graphite, this value is slightly shifted to larger values, but still lower compared to nanocrystalline graphite at ~1600 cm^{-1} [37]. This indicates the existence of nanocrystalline domains in the material combined with an amorphous carbon phase. The presence of an amorphous carbon phase is supported by the broad transition between the D- and G-mode, leading to a broad signal at ~1520 cm^{-1}. The existence of nanocrystalline carbon is demonstrated by the large I_D/I_G areal intensity ratios with similar values between 1.8 for CB3 and 2.1 for CB1 [37]. TEM shows small parts with a nanocrystalline nature for CB2 and CB3, whereas CB1 is mostly characterized by disordered carbon and only few crystalline areas (Fig. 2). The Raman spectra for the two activated carbons (AC1 and AC2) present a similar I_D/I_G ratio of 2.1 and 2.2, indicative for nanocrystalline carbon [37]. The nanocrystalline nature of the materials is also shown by TEM, with small crystalline parts connected by disordered carbon, which is in agreement with literature [38].

Using Raman spectroscopy and TEM, we can assign the highest degree of carbon ordering to EX-G [35]. Among the carbon blacks, CB1 presents the lowest degree of carbon ordering with distinct bond-length variation and distortion. Both AC materials show a distinct nanocrystalline nature indicated by a G-mode slightly smaller than 1600 cm^{-1} (nanocrystalline carbon), but smaller FWHMs of the G-mode than CB. Thus, both activated carbons present a higher degree of carbon ordering than the carbon blacks but lower than exfoliated graphite (EX-G).

The nitrogen sorption isotherms show a characteristic type I(a) shape for AC1 and type I(b) for AC2, which is related to microporous materials with pores smaller than 1 nm or 2.5 nm, respectively [39], with BET-SSA of 1681 $m^2 g^{-1}$ (QSDFT-SSA 1560 $m^2 g^{-1}$) for AC1 powder and a larger surface area for AC2 with BET-SSA of 2347 $m^2 g^{-1}$ (QSDFT-SSA 1756 $m^2 g^{-1}$). CB1 and CB2 display a mixture of type I(b) isotherm, related to the internal microporosity, and type IV(b) isotherm (mesopores) with a slight H4 hysteresis indicative of a predominantly microporous and mesoporous material and QSDFT-SSA of 1272 $m^2 g^{-1}$ and 715 $m^2 g^{-1}$, respectively (Fig. 1C) [39]. The isotherms of CB3 and EX-G are characteristic for non-porous carbons with very low SSA of less than 100 $m^2 g^{-1}$ (Fig. 1C and Table 2) with a type II shape and a H3 hysteresis. The very high nitrogen adsorption of CB1 with a specific pore volume of 1.92 $cm^3 g^{-1}$ is related to its high internal porosity and the large

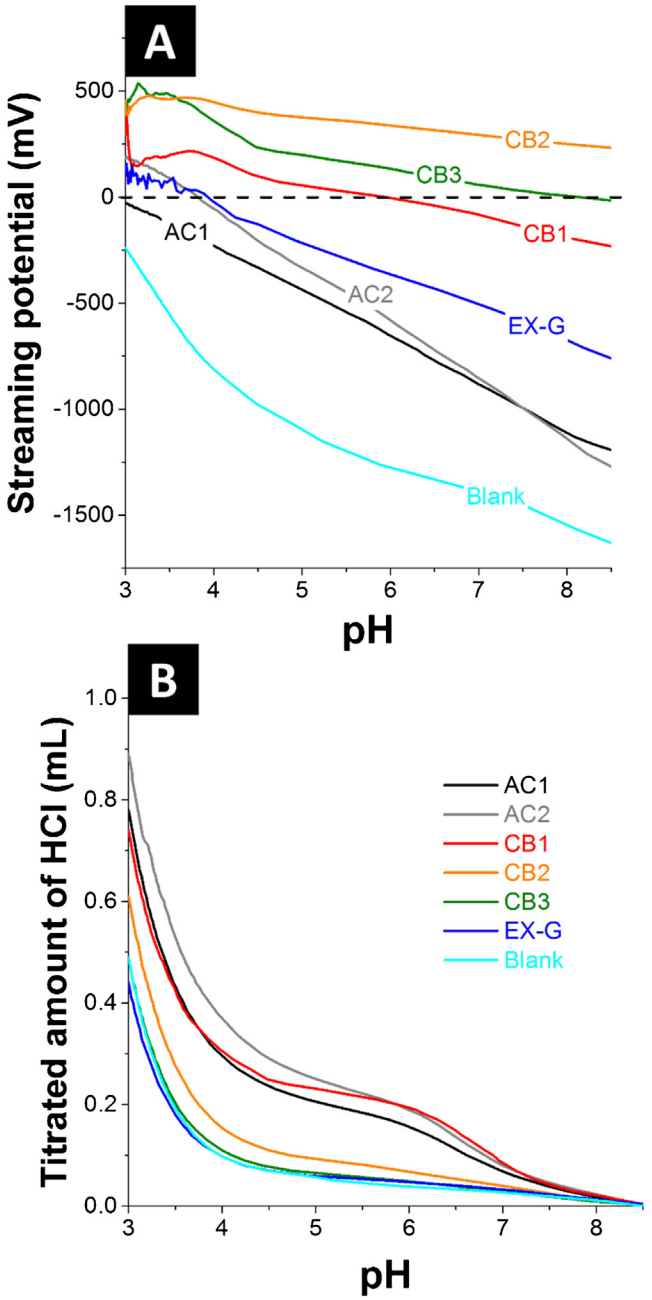

Fig. 3. (A) Streaming potential of all used carbons in pH range from 9.5 to 3 with isoelectric point at potential zero and (B) amount of needed HCl solution to set the pH value.

amount of interparticle voids due to the primary particle size of about 50 nm, as shown by TEM (Fig. 2). The same effect can be seen for CB2. The primarily microporous AC samples show the same amount of (ultra) micropores, as seen from CO_2 sorption data (Fig. 1D), but AC2 has much more micro-mesopores in the range of 1.5-5 nm in contrast to AC1. As shown in Table 2, this is a result of the higher total SSA and a much higher pore volume (1.15 $cm^3 g^{-1}$) of AC2 (1756 $m^2 g^{-1}$ QSDFT-SSA) versus AC1 (1560 $m^2 g^{-1}$ QSDFT-SSA, 0.78 $cm^3 g^{-1}$).

EDX measurements confirm the presence of oxygen, as seen from the data shown in Table 3. Two groups of materials are distinct with respect to oxygen content, namely very pure carbons like CB3 and EX-G with more than 98 atom% carbon, and the other samples with higher amount of oxygen. Oxygen in carbon materials is mainly resulting from the oxygen containing surface groups. The nature of the latter can be investigated by streaming potential measurements. One can see a high amount of acidic groups (carboxylic, lactonic, and phenolic) on AC1, AC2, and EX-G, indicated by the negative potential in the measured pH range from 8.5 to 3 and an isoelectric point below 4 (Fig. 3A and B). These acidic groups are protonated at low pH values (pH 3-5) and loose a proton by increasing the pH to neutral and basic regimes, resulting in a negative surface charge of the carbon [40]. The data for CB1 show the smallest variation in potential values ranging from +250 mV to -250 mV in the measured pH range and an isoelectrical point at neutral pH 6 (Fig. 3A). The high SSA carbons AC1, AC2, and CB1 have also the highest HCl uptake to decrease the pH value from 8.5 to 3 in contrast to the low SSA carbons CB3 and EX-G, which are very close to the uptake of the blank probe (Fig. 3B). The total amount of surface groups seems to be related to the total SSA of the material (Table 2) [41]. The streaming potentials of CB2 and CB3 have an isoelectrical point at pH 8.5 or higher and the values gradually increase to about 500 mV at pH 3 (Fig. 3A). The positive streaming potential in the acidic range ($pH < 7$) is indicative for alkali groups like carbonyl groups and these groups accept another proton in acidic regime. The settle point at ~pH 6 in Fig. 3B is related to the neutralization of NaOH with HCl.

3.2. Density, electrical conductivity, and pore size analysis of electrodes

The effective film electrode density was determined for 5 mass% PTFE-bound electrodes after compaction (Fig. 4A and C). Without any conductive additive, the density of free standing AC electrodes differs greatly: 629 ± 4 mg cm^{-3} for AC1 and 439 ± 7 mg cm^{-3} for AC2. The major difference in density is related to the much higher pore volume of AC2 in contrast to AC1 (Table 2). The electrode density remains constant when admixing CB3 or EX-G to AC1 in the range of 624-639 mg cm^{-3} (Fig. 1A). For admixture of CB1, the electrode film density decreases by 5-10% to values of 569-601 mg cm^{-3} since CB1 forms big agglomerates and the filling of void volume does not occur. The electrode density increases in case of CB2 to 710 mg cm^{-3} for 10 mass% CB2 in AC1 (Fig. 4A). This increase might be related to a unique fitting of CB2 particles in AC1 interparticle voids, supported by the absence of agglomerate formation in ethanol by centrifugation analysis (Fig. 1A); by this virtue, CB2 can effectively fill the void volume between the AC particles in contrast to all other additive particles. For AC2 and any admixture of conductive additives, the electrode density remains fairly constant with values from 425 mg cm^{-3} to 447 mg cm^{-3} (Fig. 4C).

The electrical sheet resistance (Fig. 4B and D) can be significantly improved when admixing a conductive additive to AC film electrodes (AC1: $11.4 \pm 1\ \Omega$ cm, AC2: $9.0 \pm 0.5\ \Omega$ cm). Compared to AC electrode films, electrodes composed only of the conductive additive (with 10 mass% PTFE) show a much lower electrical resistance of 0.3–0.9 Ω cm (Fig. 4B and D, 100%). All conductive additives show a comparable trend of reduced resistance with increased loading with conductive additive. For quite all additives, there is a drop in sheet resistance of 25-35% with 2.5 mass% additive content. This can be explained by high intrinsic conductivity of the additives and by a larger number of particle-particle-contacts, resulting in a higher carbon-carbon contact area. Especially, CB2 admixture to AC1 at 2.5 mass% additive content strongly reduces the sheet resistance from $11.4 \pm 1\ \Omega$ cm (constituent AC1) to $3.1 \pm 0.3\ \Omega$ cm with a 5%

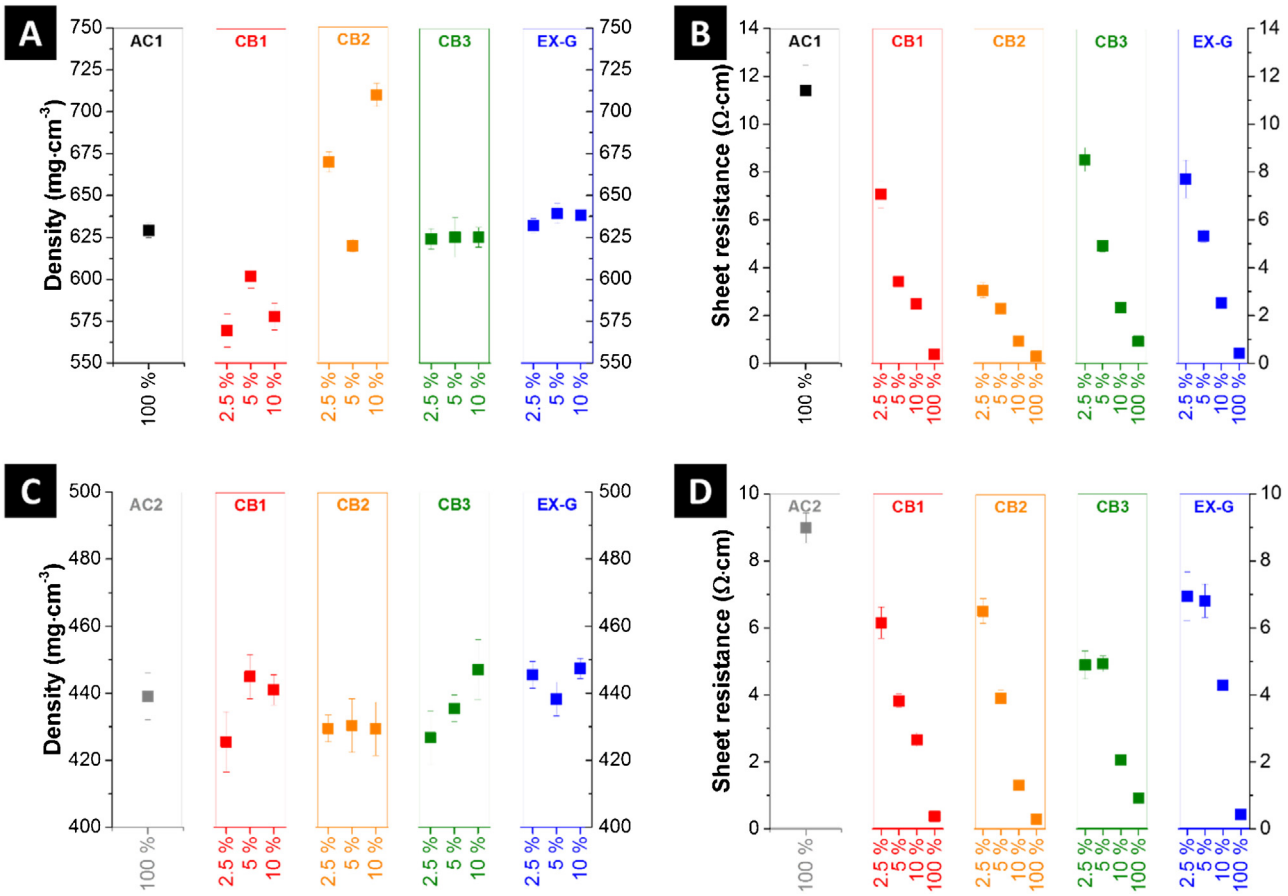

Fig. 4. Density of PTFE-bound composite electrodes with conductive additive admixture in (A) AC1 matrix and (C) AC2 matrix. Sheet resistance of the used composite electrodes with (B) AC2 and (D) AC1. The amount of additive admixture is displayed with the numbers on the *x*-axis. "100%" for AC1 and AC2 refers to the sample with constituent activated carbon (i.e., no conductive additive).

Table 4
Specific surface area of electrodes (BET-SSA and QSDFT-SSA), pore volume and average pore size of all used materials and composites. All values in percent are related to mass-percent. The average pore size denotes the volume-weighed pore size average.

Material	BET SSA ($m^2 g^{-1}$)	QSDFT SSA ($m^2 g^{-1}$)	Pore volume ($cm^3 g^{-1}$)	Average pore size (nm)
AC1 + 5% PTFE	1481	1320	0.67	0.8
AC1 + 2.5% CB1 + 5% PTFE	1392	1302	0.64	1.6
AC1 + 5.0% CB1 + 5% PTFE	1422	1357	0.69	1.0
AC1 + 10% CB1 + 5% PTFE	1403	1357	0.74	1.2
AC1 + 2.5% CB2 + 5% PTFE	1374	1321	0.61	0.9
AC1 + 5.0% CB2 + 5% PTFE	1342	1308	0.64	1.0
AC1 + 10% CB2 + 5% PTFE	1100	1085	0.53	1.0
AC1 + 2.5% CB3 + 5% PTFE	1432	1281	0.71	0.9
AC1 + 5.0% CB3 + 5% PTFE	1355	1356	0.64	0.9
AC1 + 10% CB3 + 5% PTFE	1287	1260	0.61	0.9
AC1 + 2.5% EX-G + 5% PTFE	1445	1317	0.68	0.9
AC1 + 5.0% EX-G + 5% PTFE	1408	1298	0.65	0.9
AC1 + 10% EX-G + 5% PTFE	1277	1300	0.62	0.9
AC2 + 5% PTFE	2105	1672	1.01	1.6
AC2 + 2.5% CB1 + 5% PTFE	1864	1496	0.90	1.6
AC2 + 5.0% CB1 + 5% PTFE	1940	1522	0.98	1.8
AC2 + 10% CB1 + 5% PTFE	1987	1587	1.00	2.0
AC2 + 2.5% CB2 + 5% PTFE	1948	1565	0.98	1.4
AC2 + 5.0% CB2 + 5% PTFE	1912	1496	0.96	1.4
AC2 + 10% CB2 + 5% PTFE	1881	1531	0.94	1.4
AC2 + 2.5% CB3 + 5% PTFE	1962	1506	1.03	1.4
AC2 + 5.0% CB3 + 5% PTFE	1924	1493	1.01	1.4
AC2 + 10% CB3 + 5% PTFE	1773	1363	0.94	1.5
AC2 + 2.5% EX-G + 5% PTFE	1808	1435	0.88	1.3
AC2 + 5.0% EX-G + 5% PTFE	1803	1429	0.91	1.3
AC2 + 10% EX-G + 5% PTFE	1606	1253	0.79	1.4

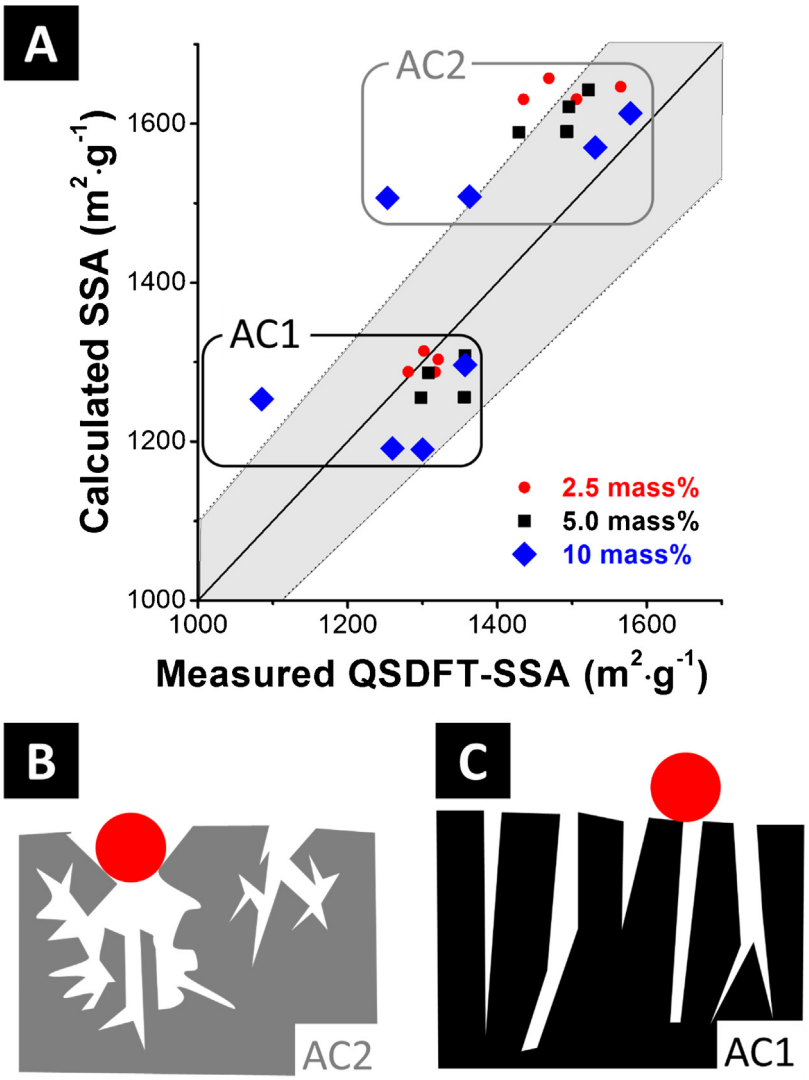

Fig. 5. (A) Parity plot of all composite electrodes with measured QSDFT-SSA versus calculated SSA, which is linear addition of constituent SSA measurements. (B) Scheme of the hierarchical pore size distribution of AC2 with an additive particle blocking the entrance to smaller pores. (C) Scheme of the slit-like pores of AC1, whereas the pore blocking does not diminish the total SSA of the composite.

increase in electrode density. This supports the statement with a unique fitting of CB2 within the AC1 particle matrix. The percolation of additive particles in AC seems to depend strongly on the structure of particle shape and interparticle voids of AC and the agglomerate size of the used additive.

The presence of polymer binder in composite electrodes impacts on the ion-accessible surface area and pore volume [42]. The QSDFT-SSA values are significantly lower for film electrodes containing 5 mass% PTFE compared to the QSDFT-SSA of the powders without binder with a decrease of 5-18% (Tables 2 and 4). This effect is caused by pore blocking [43], but also the mere presence of binder, which basically is dead mass with a surface area of less than 5 $m^2 \cdot g^{-1}$ (see Ref [42]). Roughly, we can attribute a 5% decrease in QSDFT-SSA just due to the presence of 5 mass% of polymer binder without additionally considering pore blocking.

The pore blocking effect by PTFE and the influence of conductive additive particles on the total SSA of the electrodes was calculated by assuming a mechanical rule-of-mixture (Fig. 5). This enables us to plot calculated values for an ideal mechanical mixture via linear addition of constituent carbon electrodes calculated values (e.g., 0.95·AC1-SSA + 0.05·CB1-SSA = calculated value of AC1 + 5% CB1) versus the experimentally measured SSA of the electrodes for different amounts of conductive additive admixture (data also provided in Table 4). As seen from Fig. 5, most of the values fall within a ±10% error margin (grey box) compared to the ideal case (parity line = solid line) what is an average error supposed on nitrogen sorption derived data. The outliers are all related to AC with admixture of EX-G. The inhomogeneous distribution is related to the large flake size (Fig. 1A) and the low amount of tested electrode film (approx. 10 mg) as well as the very different SSA of AC and EX-G can explain the larger difference between calculated value and measured sample. Nevertheless, in case of AC1 many points remain below the parity line (measured SSA is larger than calculated SSA) in contrast to the points of AC2 which are mostly above the parity line (measured SSA is smaller than calculated SSA). A smaller measured SSA than calculated can be explained with pore blocking. For AC2 with a wider pore size distribution and

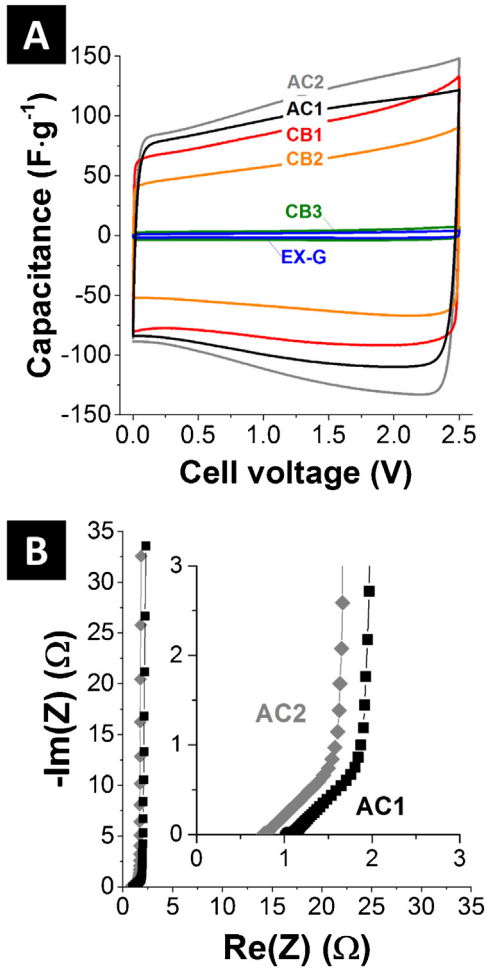

Fig. 6. (A) CVs of constituent carbon electrodes at 10 mV s^{-1} in 1 M TEA-BF_4/ACN. (B) Nyquist plot of electrical impedance spectroscopy with two activated carbon electrodes in 1 M TEA-BF_4/ACN. Inset shows the enlarged plot at low resistance.

more hierarchical pores the additive particles can block the entrance to several smaller pores and a lot of surface of the AC particle is no longer available (Fig. 5B). Since AC1 has only long, uniform and slit-like pores the pore blocking also occurs but there is only a very small amount of SSA blocked by the additive particle and the total SSA of the composite electrode is not diminished (Fig. 5C).

3.3. Electrochemical behavior and rate capability

Cyclic voltammetry (CV) in symmetrical full cells was carried out first on all constituents, without mixing AC and conductive additives. The measured CVs show all a rectangular shape at low scan rates (10 mV s^{-1}) in 1 M TEA-BF_4/ACN (Fig. 6A). Both AC materials yield a more pronounced resistive behavior compared to electrodes only composed of conductive additive, as seen by the presence of a resistive knee in the CVs. The characteristic increase in current at higher voltage, resulting in the so-called "butterfly" shape and an increase in differential capacitance, is a result of the increase in density of states (DOS) [27,44,45]. The electrical impedance spectra show a similar behavior of both ACs, whereas the slightly higher degree of carbon ordering of AC2 (I_D/I_G ratio = 2.1) results in a lower electrical series resistance (ESR) [2] compared to AC1. In addition, both ACs show roughly the same EDR (equivalent distributed resistance) [2]. which is particularly characteristic in predominately microporous carbon materials where electrolyte ion penetration becomes a limiting factor [22]. As shown in Fig. 1D, the (ultra) micropore structure is equal for both ACs and this results in equal EDR values. Moreover, both curves end up at the same resistance what is related to an equal thickness of electrodes (Fig. 6B).

As a next step, we investigated the electrochemical performance when admixing discrete amounts of conductive additive (i.e., 2.5, 5.0, and 10 mass%) to both AC materials. Four different conductive additive are added to the two activated carbons (Fig. 7). The rate capability was evaluated by GCPL from 0.1 A g^{-1} to 10 A g^{-1} and the performances at these two specific currents are shown in Fig. 7. The data shows that AC1 and AC2 exhibit a clear trend at low specific current of 0.1 A g^{-1}: adding any amount of any of the investigated conductive additives causes a decrease in specific capacitance (Fig. 7A and C). This is related to the effective reduction in total pore volume of the film electrodes when mixing high surface area AC with conductive additives having a lower porosity. When only using activated carbon, the film electrodes yield at lowest specific current a specific capacitance of 104 F g^{-1} (AC1) or 112 F g^{-1} (AC2), in agreement with the higher surface area of the latter. The general trend is that higher amounts of admixture reduce the specific capacitance even further whereas the decrease in specific capacitance is more significant for AC2 compared to AC1.

The situation changes at a high specific current of 10 A g^{-1} (Fig. 7B and D). As a baseline, AC1 without any additive yields a specific capacitance of 71 F g^{-1} and AC2 of 81 F g^{-1}. The lower relative loss in capacitance compared to the low specific current performance for AC2 (i.e., -32%,) is related to the lower sheet resistance conductivity (9.0 Ω cm) in comparison with AC1 (71 F g^{-1}; i.e., −28%, 11.4 Ω cm, I_D/I_G = 2.2). In contrast, composite electrodes containing additives can deliver up to 87 F g^{-1} in case of 2.5% CB2 admixture (Fig. 7B).

From these data, two general conclusions can be drawn: (1) A capacitance drop of 4–10% at 0.1 A g^{-1} appears by comparison of constituent AC electrode with conductive additive composite electrodes (Fig. 7A and C) and (2) the smallest capacitance loss for composite electrodes occurs only with certain admixture of conductive additive at high loads. Thus, conductive additives are only useful at high specific currents (Fig. 7B and D). This fact has also been shown for onion-like carbon (OLC) or graphene-based additives [18,46].

The equilibration time until the final state of ion (re) distribution within the pore network of micrometer-sized AC particles pores is rather long at low specific current [47]; this process is much faster in nanometer-sized porous carbons [48] or non-porous [49] nanoparticles where double-layer formation occurs only on the outer surface. For better comparability, the specific capacitance of either AC1 or AC2 at either 0.1 A g^{-1} or 10 A g^{-1} has been set to zero in Fig. 8 and only the deviation ΔC in% of the constituent AC electrode performance is shown. This way, it is easier to see if adding a conductive additive increases or decreases the specific capacitance. When comparing the performance of just AC1 or AC2 with electrodes containing conductive additive admixtures, one can see a decrease of 2-17% of the specific capacitance at 0.1 A g^{-1} (Fig. 8A and C). Especially for AC2 we see a particularly strong decrease about 5-17% of the electrochemical performance when adding any conductive additive (Fig. 8C) which is related to the pore blocking phenomenon as described in Fig. 5. At high specific currents (10 A g^{-1}), the situation is more complex and while some additives at some admixture contents still decrease the performance, there are several important exceptions. For example, there is an increase in capacitive retention of more than 20% for the system AC1 + 2.5 mass% CB2

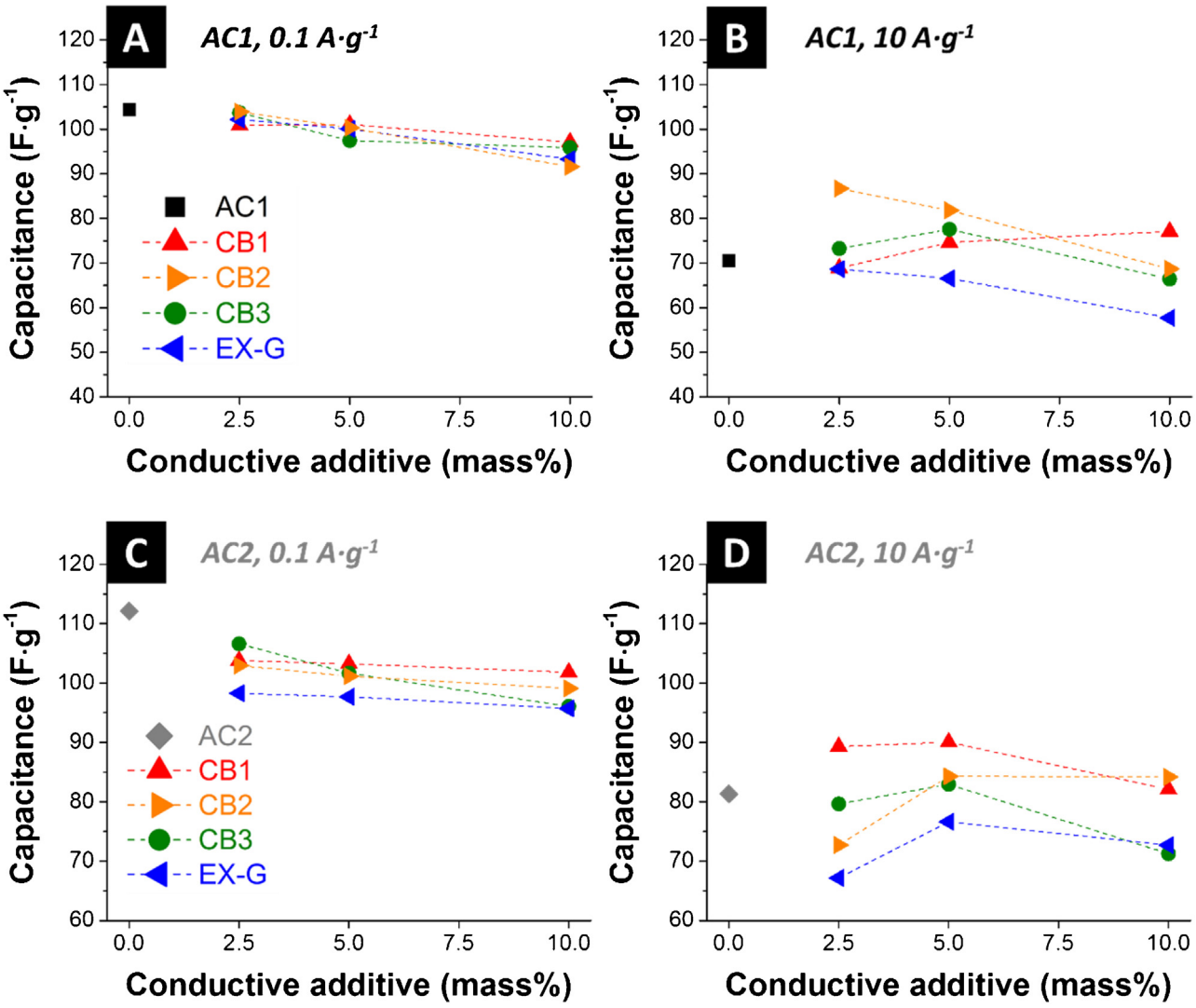

Fig. 7. Rate capability measurements of all composite electrodes with (A and C) a low rate of 0.1 A g^{-1} and (B and D) with a high rate of 10 A g^{-1}. The *x*-axis shows the amount of used conductive additive in the AC matrix of (A and B) AC1 and (B and D) AC2. "0%" is related to constituent AC electrode. The color and symbol chart given in panel A and C also relate for panel B and D, respectively.

(Fig. 8B), whereas the maximum enhancement of AC2 is 11% with the mixture AC2 + 5 mass%CB1.

The different effects of the conductive additives can be rationalized by considering the influence of agglomerate size (Fig. 1A) and the effective percolation level within the AC particle matrix. Furthermore, the intrinsic behavior of each carbon material, like SSA (Table 2), density, and surface functional groups, has to be taken into account. For example, when mixing AC1 and CB1, we see a continuous improvement of the electrochemical performance with higher additive content related to the high SSA of CB1 (powder: 1272 $m^2 g^{-1}$) and its high electrical conductivity (Fig. 4B). For this system, there is only a minor loss in total SSA of the electrode (Table 4) and it can be assumed that the highly conductive particles form a percolated network at a concentration of around 5 mass% in AC1. For CB2 with moderate SSA (powder: 715 $m^2 g^{-1}$) we see a continuous decrease in electrode capacitance when increasing the amount of additive to more than 2.5 mass% in AC1 (Fig. 8B). This effect is due to the small agglomerate size (d_{90} = 0.2 μm), resulting in a homogenous distribution of CB2 even at a very low amount (i.e., the percolation threshold is reached at low concentration of CB2). In case of CB3, a maximum capacitive enhancement is seen when admixing 5 mass% either to AC1 (+7.1 F g^{-1} at 10 A g^{-1},Fig. 8B) or AC2 (+1.6 F g^{-1} at 10 A g^{-1}, Fig. 8D). A homogeneous distribution of all used CB particles in-between AC grains reduces the overall contact resistance effectively (Fig. 4B and D). Any further increase of the amount of conductive additive particles beyond 5 mass% decreases the total electrode SSA and leads to a decreased overall supercapacitor performance, while the electrical conductivity of the composite electrode still improves.

In contrast to CB, admixing graphite flakes never yielded any improvement in the electrochemical performance. We explain this effect by the very large particle size of EX-G and its very low SSA. It can be assumed that the two-dimensional in-plane conductivity of EX-G cannot decrease the interparticle resistance as effectively as a three-dimensional network of highly conductive graphitic shells of carbon blacks. Seemingly, the carbon-carbon contact area can be effectively increased by using spherical carbon additives with a small aggregate size to ensure a homogeneous distribution in the AC particle matrix.

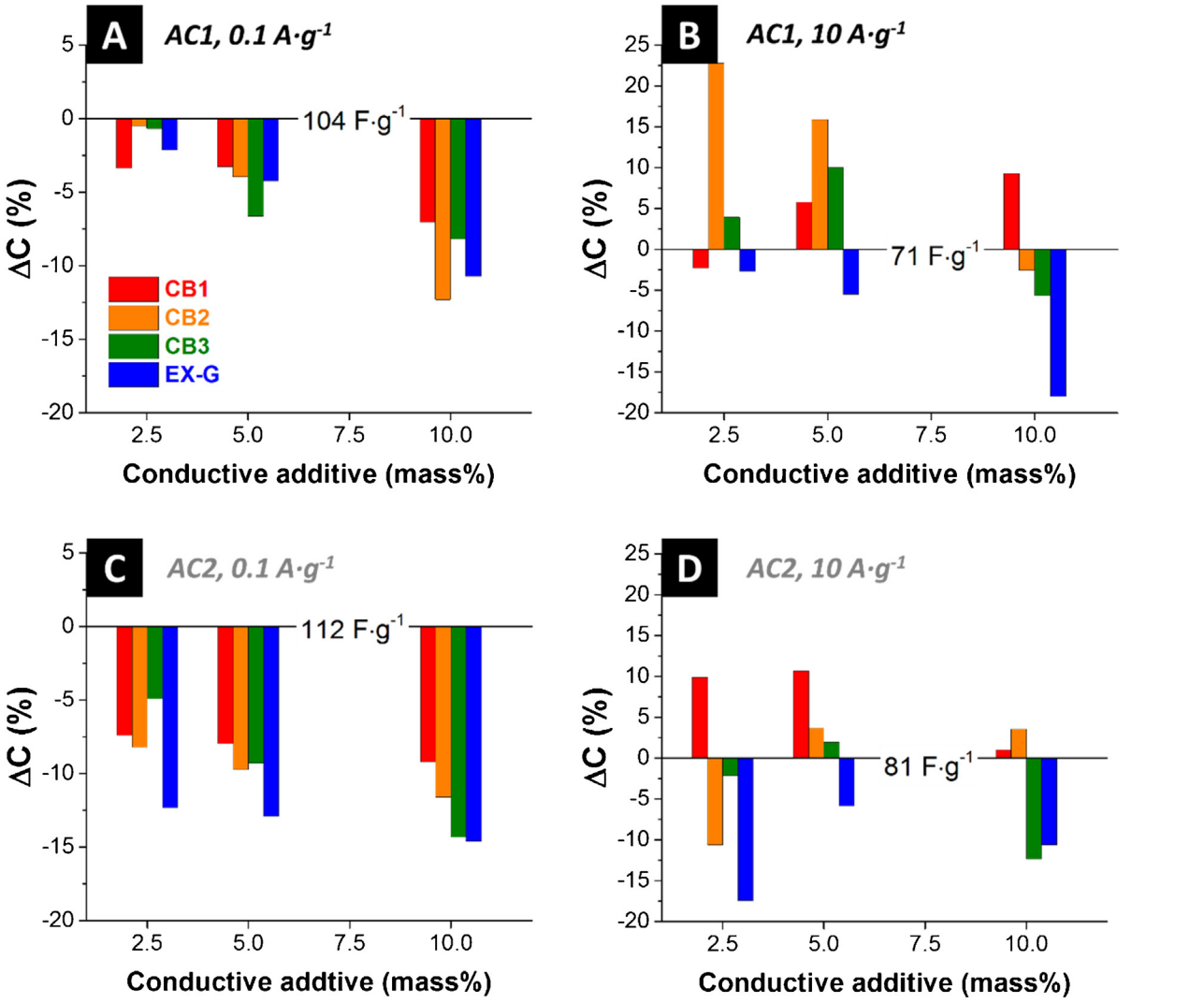

Fig. 8. Gain (positive values) or loss (negative values) of specific capacitance for conductive additive composite electrodes in comparison to performance of constituent AC electrodes (A and C) at a low rate of 0.1 A g^{-1} and (B and D) at a high rate of 10 A g^{-1}. The black line (and the value) marks the performance of a constituent AC full cell. The color code in panel (A) relates to all panels.

3.4. Long-time performance testing by voltage floating

Long-time performance evaluation was carried out at 2.7 V in a symmetrical full cell for 100 h. Voltage floating enables demanding benchmarking and is commonly employed in industry [23]. This method yields stable performance over long floating time when subjecting AC electrodes to a cell voltage of 2.75 V in 1 M TEA-BF_4/ACN with less than 30 ppm of water [24]. Floating test has proven as more demanding test compared to cycling in the same voltage window because the floating test delivers clear results in less time [23]. First, we investigated the performance stability for AC1 and admixtures to AC1. In Fig. 9, we see a decrease in capacitance of 6.2% for AC1 after 100 h. Admixing any amount of any of the studied additives decreased the performance stability over time; yet, the performance stability of any of the conductive additives constituently was very high yielding a decrease in capacitance below 5% after 100 h of voltage floating. The only exception: admixing CB2 to AC1 (Fig. 9B) slightly increases the floating performance stability (+2% for 2.5 mass% CB2 in AC1), but any further increase of CB2 amount also decreases the performance as described before. Adding CB3 to AC1 (Fig. 9C), the capacitive retention after 100 h is always below that of either only AC1 or only CB3. The data also show that different amounts of CB3 admixture barely influence the performance and the same effect can be seen when adding EX-G (Fig. 9D).

Next, we investigated the same set of conductive additive admixtures and their influence on the long-time stability of AC2-based electrodes. The results are very similar to the data set of AC1 (Fig. 10). However, the performance of constituent AC2 (89% retention after 100 h floating test) is lower than for AC1 (94% after 100 h). Especially the admixture of CB2 into AC2 matrix decreases the long-time stability tremendously: already after 10 h of voltage

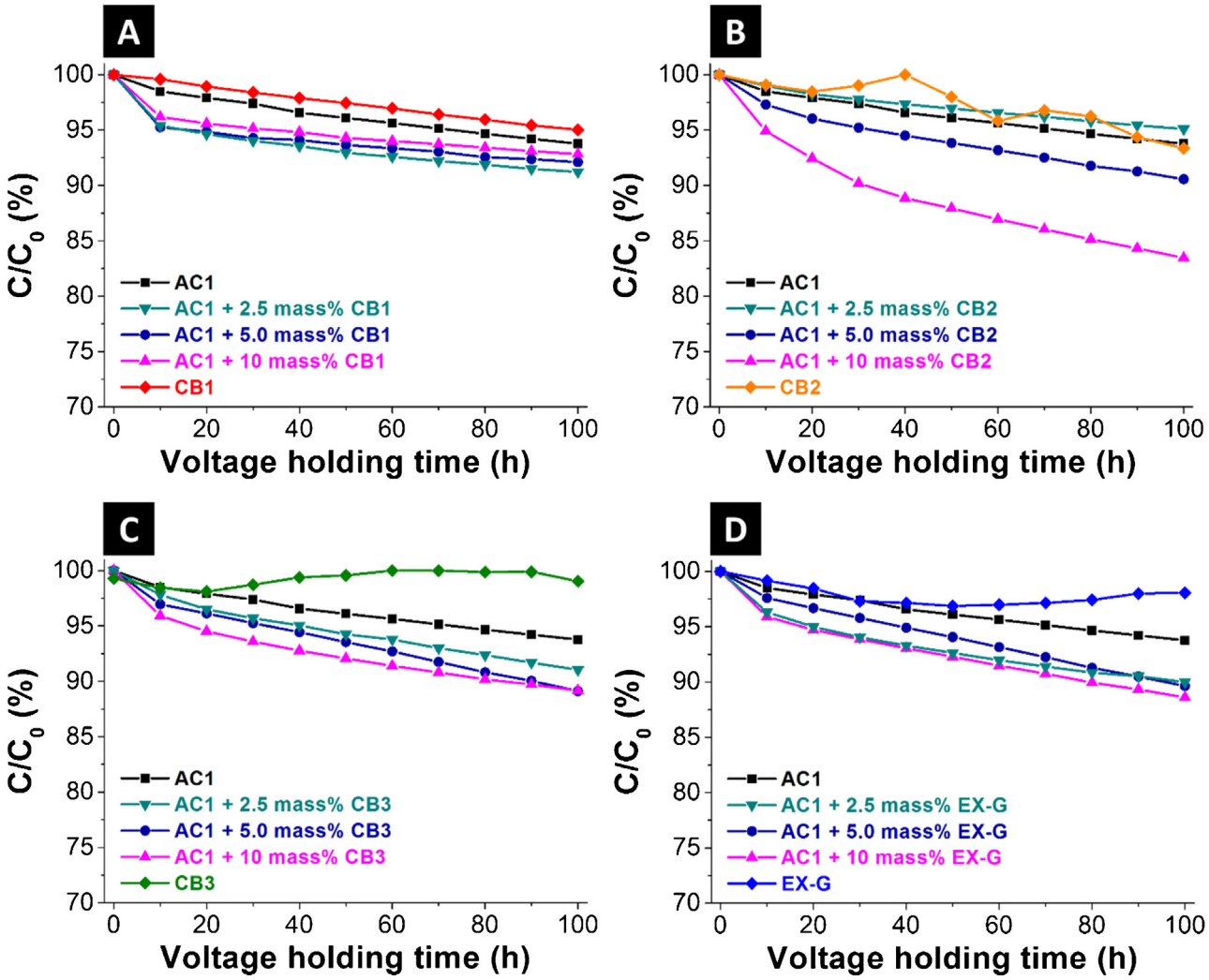

Fig. 9. Long-time floating stability testing at 2.7 V for AC1 with (A) admixture of CB1, (B) admixture of CB2, (C) admixture of CB3, and (D) admixture of EX-G. The amount of additive is 0 mass% (i.e., pure AC1), 2.5 mass%, 5 mass%, or 10 mass%.

floating, the retention drops to 80% C/C_0 when adding 10 mass% CB2.

The decrease in longevity of AC electrodes when using a composite electrode containing activated carbon and conductive additive is surprising, especially when considering the excellent stability for either just AC or just the conductive additives. The exact mechanism of this behavior remains unclear at the moment. A possible mechanism explaining the decrease in long-time performance for composite electrodes may relate to the combined presence of acidic and alkaline surface groups. The highly acidic surface groups, for example of AC1 (Fig. 3A), may react with the mostly alkaline groups of CB2 at an elevated potential of 2.7 V during voltage floating. This leads to an exchange of protons and the possible production of free water molecules, especially at the contact area of both types of carbon, with a deteriorating effect on the stability of acetonitrile near the electrode surface [50].

With the limited detectability of degradation products by post mortem analysis in the electrolyte itself, we investigated chemical changes of the aged electrodes by EDX to gain further insights (Fig. 11). Electrochemical decomposition of TEA-BF_4/ACN forms (fluoro) acetic acid, as well as acetamide, depending on the concentration of free water in the electrolyte, and free water is generated by condensation of amino-carbonyl compounds. Moreover, the corrosion (i.e., hydrolysis) of the BF_4 ion produces free fluorine atoms which like to react with protons to produce HF and this is further accelerating the decomposition of the electrolyte [51]. These processes severely affect the long-time stability, as shown by Cericola et al. [52]. For our system, we cannot identify these degradation products via the boron signal considering the very strong signal intensity of carbon. Thus, we can use for aged and thoroughly ACN rinsed electrodes the fluorine signal coming from F trapped at the surface from reactions and decomposition of the BF_4 [51]. The fresh composite electrode after contact with electrolyte (AC2 + 10 mass% CB2 + 5 mass% PTFE) showed a constant and omnipresent fluorine signal across the scanned area related to the PTFE binder. In fact, we did not find any significant increase in the measured fluorine signal even when mapping the ultrathin PTFE fibrils seen in the SEM micrographs, whereas the aged positive electrode shows certain regions with much higher

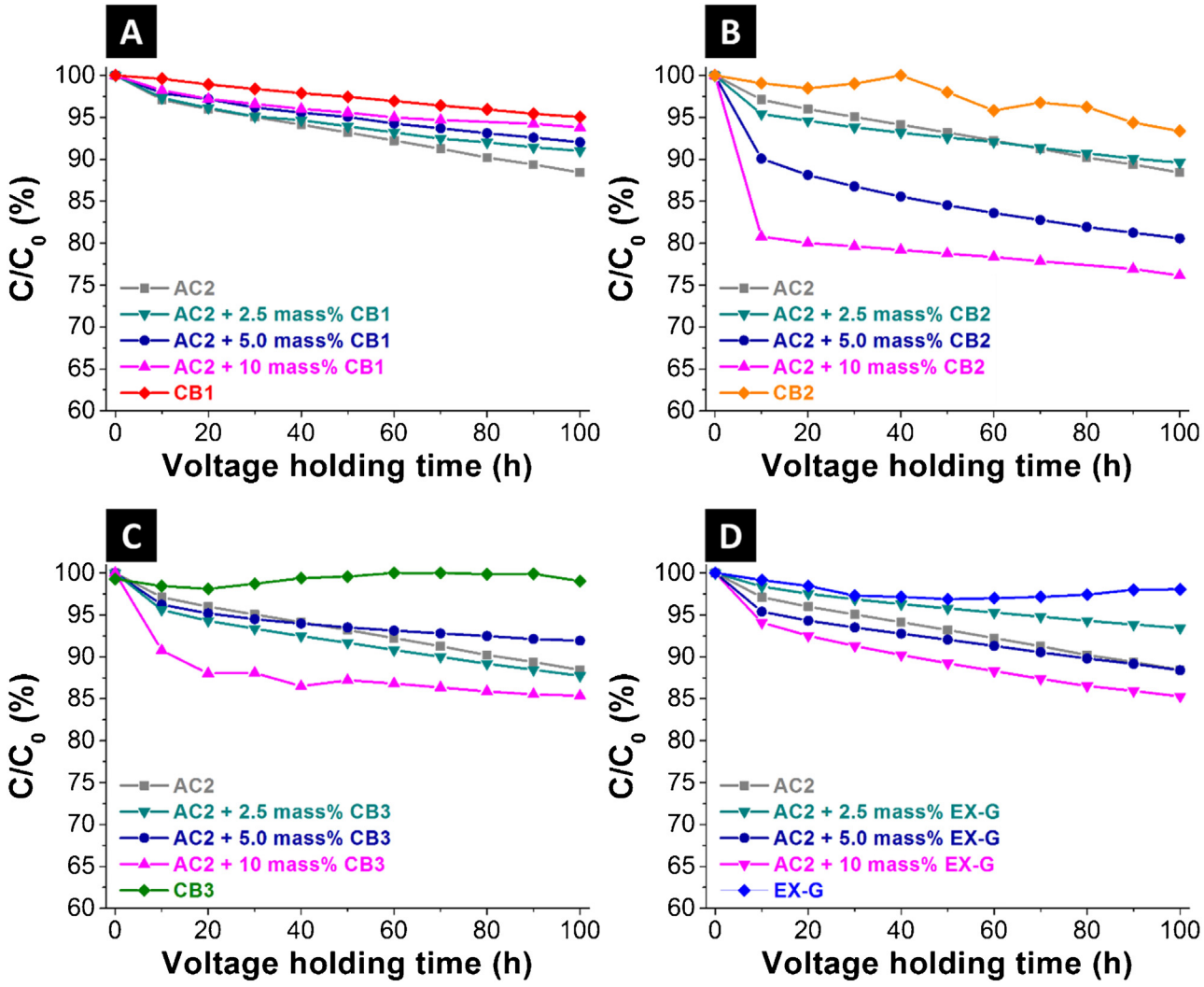

Fig. 10. Long-time floating stability testing at 2.7 V for AC2 with (A) admixture of CB1, (B) admixture of CB2, (C) admixture of CB3, and (D) admixture of EX-G. The amount of additive is 0 mass% (i.e., pure AC2), 2.5 mass%, 5 mass%, or 10 mass%.

fluorine signal. Some slight variations in the total signal strength only occurred in relation to the particle shape and morphology. However, reproducibly and significantly at contact between CB2 and AC2, we found an increase of fluorine (Fig. 11A) which was absent for the non-aged mixture (Fig. 11D). We assume this is related to the decomposition of the electrolyte at the interface between activated carbon and conductive additive where the exchange of protons is possible at elevated potential. The trace water may, accordingly, act as a catalyst for the decomposition of the electrolyte.

The implication of a decreased electrochemical performance longevity when adding conductivity certain conductive additive is of high importance for industrial applications and needs to be considered accordingly.

4. Conclusions

We present a comprehensive study of two activated carbons and four conductive additives with structural, chemical, and electrochemical measurements. The conductive additives were admixed in certain amounts and the electrochemical performance was evaluated in laboratory size cells via rate handling testing up to 10 A g^{-1} and voltage floating over 100 h in a standard organic electrolyte (1 M TEA-BF_4 in ACN). A decreased sheet resistance for an increased amount of conductive additive does not necessarily translate to an improved rate handling. Especially at low rates, the gravimetric capacitance drops generally after adding carbons with low SSA to AC. However, the rate performance can be increased up to 20% at 10 A g^{-1} by optimizing the amount of conductive particles to AC (in our study between 2.5-5 mass%). The long-time stability via voltage floating of composite electrodes is always inferior to electrodes composed of either AC or the conductive additive materials. In our study we explain this effect with the generation of water at the electrolyte-electrode interface by mixing alkaline and basic surface groups from different carbons. We demonstrate for the first time that mixing acidic and basic carbon materials leads also to a deterioration of long-time performance, especially at the contact area of basic and alkaline decorated surfaces. Thus, further work will have to investigate this effect in more detail.

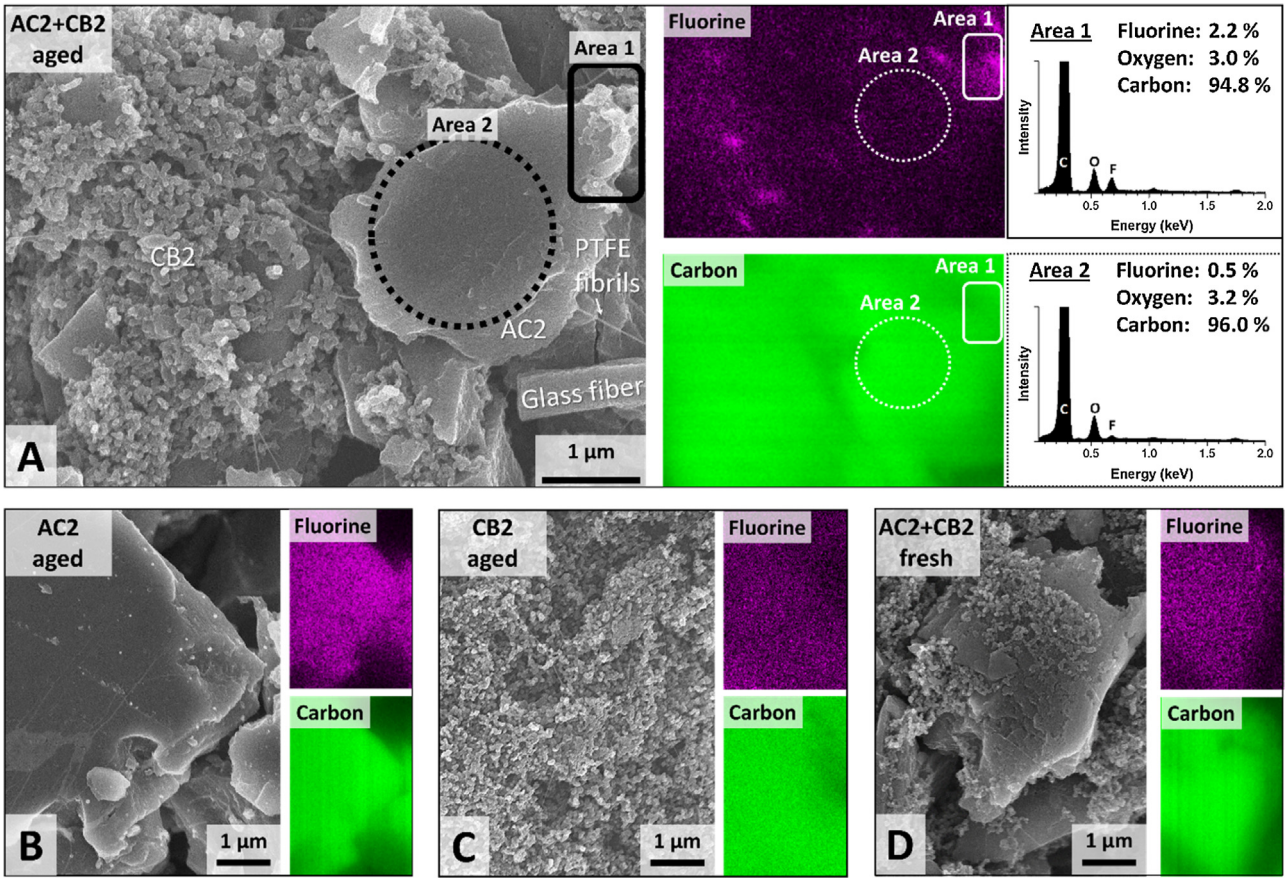

Fig. 11. SEM micrographs and EDX mapping for fluorine and carbon of (A) aged composite electrode AC2 + 10% CB2 + 5% PTFE (AC2 + CB2 aged), (B) aged activated carbon electrode AC2 + 5% PTFE, (C) aged carbon black electrode CB2 + 10% PTFE, (D) and non-aged (fresh) composite electrode AC2 + 10% CB2 +5% PTFE.

Acknowledgements

We thank Imerys Graphite & Carbon, Switzerland, for kindly providing the additives Ensaco350, C65, and the experimental expanded graphite. We acknowledge funding from the German Federal Ministry for Research and Education (BMBF) in support of the nanoEES^{3D} project (award number 03EK3013) as part of the strategic funding initiative energy storage framework. We also acknowledge additional funding via the INM FOCUS project IZIcap and thank Prof. Eduard Arzt (INM) for his continuing support.

References

[1] A. Burke, Ultracapacitors: why, how, and where is the technology, Journal of Power Sources 91 (1) (2000) 37–50.
[2] R. Kötz, M. Carlen, Principles and applications of electrochemical capacitors, Electrochimica Acta 45 (15–16) (2000) 2483–2498.
[3] A.G. Pandolfo, A.F. Hollenkamp, Carbon properties and their role in supercapacitors, Journal of Power Sources 157 (1) (2006) 11–27.
[4] M. Lu, F. Beguin, E. Frackowiak, Supercapacitors: Materials, Systems and Applications, Wiley, 2013.
[5] B.E. Conway, Electrochemical Supercapacitors: Scientific Fundamentals and Technological Applications, Springer, 1999.
[6] D. Aurbach, Review of selected electrode-solution interactions which determine the performance of Li and Li ion batteries, Journal of Power Sources 89 (2) (2000) 206–218.
[7] C. Liu, et al., Advanced materials for energy storage, Adv Mater 22 (8) (2010) E28–62.
[8] P. Simon, Y. Gogotsi, Materials for electrochemical capacitors, Nat Mater 7 (11) (2008) 845–854.
[9] H. Marsh, F.R. Reinoso, Activated carbon, Elsevier, 2006.
[10] J. Chmiola, et al., Desolvation of ions in subnanometer pores and its effect on capacitance and double-layer theory, Angewandte Chemie - International Edition 47 (18) (2008) 3392–3395.
[11] R. Mysyk, E. Raymundo-Pinero, F. Beguin, Saturation of subnanometer pores in an electric double-layer capacitor, Electrochemistry Communications 11 (3) (2009) 554–556.
[12] L. Zhang, et al., Controlling the effective surface area and pore size distribution of sp2 carbon materials and their impact on the capacitance performance of these materials, J Am Chem Soc 135 (15) (2013) 5921–5929.
[13] F. Beguin, et al., Carbons and electrolytes for advanced supercapacitors, Adv Mater 26 (14) (2014) 2219–2251, 2283.
[14] P.J. Hall, et al., Energy storage in electrochemical capacitors: designing functional materials to improve performance, Energy & Environmental Science 3 (9) (2010) 1238–1251.
[15] S. Zhang, N. Pan, Supercapacitors Performance Evaluation, Advanced Energy Materials 5 (6) (2015) 1401401.
[16] D. Weingarth, et al., Carbon additives for electrical double layer capacitor electrodes, Journal of Power Sources 266 (2014) 475–480.
[17] A.G. Pandolfo, et al., The Influence of Conductive Additives and Inter-Particle Voids in Carbon EDLC Electrodes, Fuel Cells 10 (5) (2010) 856–864.
[18] N. Jäckel, et al., Comparison of carbon onions and carbon blacks as conductive additives for carbon supercapacitors in organic electrolytes, Journal of Power Sources 272 (2014) 1122–1133.
[19] G.X. Wang, Z.P. Shao, Z.L. Yu, Comparisons of different carbon conductive additives on the electrochemical performance of activated carbon, Nanotechnology 18 (20) (2007) 205705.
[20] M.E. Spahr, et al., Development of carbon conductive additives for advanced lithium ion batteries, Journal of Power Sources 196 (7) (2011) 3404–3413.
[21] W. Guoping, et al., The effect of different kinds of nano-carbon conductive additives in lithium ion batteries on the resistance and electrochemical behavior of the LiCoO2 composite cathodes, Solid State Ionics 179 (7–8) (2008) 263–268.
[22] C. Portet, et al., Influence of carbon nanotubes addition on carbon-carbon supercapacitor performances in organic electrolyte, Journal of Power Sources 139 (1–2) (2005) 371–378.

[23] D. Weingarth, A. Foelske-Schmitz, R. Kötz, Cycle versus voltage hold—Which is the better stability test for electrochemical double layer capacitors? Journal of Power Sources 225 (2013) 84–88.
[24] P.W. Ruch, et al., Aging of electrochemical double layer capacitors with acetonitrile-based electrolyte at elevated voltages, Electrochimica Acta 55 (15) (2010) 4412–4420.
[25] P. Azais, et al., Causes of supercapacitors ageing in organic electrolyte, Journal of Power Sources 171 (2) (2007) 1046–1053.
[26] M. Hahn, et al., Gas evolution in activated carbon/propylene carbonate based double-layer capacitors, Electrochemistry Communications 7 (9) (2005) 925–930.
[27] D. Weingarth, et al., Graphitization as a Universal Tool to Tailor the Potential-Dependent Capacitance of Carbon Supercapacitors, Advanced Energy Materials 4 (13) (2014).
[28] D. Weingarth, et al., PTFE bound activated carbon—A quasi-reference electrode for ionic liquids, Electrochemistry Communications 18 (0) (2012) 116–118.
[29] P.W. Ruch, et al., On the use of activated carbon as a quasi-reference electrode in non-aqueous electrolyte solutions, Journal of Electroanalytical Chemistry 636 (1–2) (2009) 128–131.
[30] S. Brunauer, P.H. Emmett, E. Teller, Adsorption of Gases in Multimolecular Layers, Journal of the American Chemical Society 60 (2) (1938) 309–319.
[31] G.Y. Gor, et al., Quenched solid density functional theory method for characterization of mesoporous carbons by nitrogen adsorption, Carbon 50 (4) (2012) 1583–1590.
[32] P.I. Ravikovitch, G.L. Haller, A.V. Neimark, Density functional theory model for calculating pore size distributions: pore structure of nanoporous catalysts, Advances in Colloid and Interface Science 76 (0) (1998) 203–226.
[33] A. Vishnyakov, P.I. Ravikovitch, A.V. Neimark, Molecular level models for CO_2 sorption in nanopores, Langmuir 15 (25) (1999) 8736–8742.
[34] F. Beguin, et al., Carbons and electrolytes for advanced supercapacitors, Advanced Materials 26 (14) (2014) 2219–2251.
[35] F. Tuinstra, J.L. Koenig, Raman Spectrum of Graphite, Journal of Chemical Physics 53 (3) (1970) 1126–1130.
[36] C. Thomsen, S. Reich, Double resonant raman scattering in graphite, Phys Rev Lett 85 (24) (2000) 5214–5217.
[37] A.C. Ferrari, J. Robertson, Raman spectroscopy of amorphous, nanostructured, diamond—like carbon, and nanodiamond, Philosophical Transactions of the Royal Society of London Series A 362 (1824) (2004) 2477–2512.
[38] N. Shimodaira, A. Masui, Raman spectroscopic investigations of activated carbon materials, Journal of Applied Physics 92 (2) (2002) 902–909.
[39] M. Thommes, et al., Physisorption of gases, with special reference to the evaluation of surface area and pore size distribution (IUPAC Technical Report), Pure and Applied Chemistry 87 (9–10) (2015).
[40] S. Porada, et al., Capacitive Deionization using Biomass-based Microporous Salt-Templated Heteroatom-Doped Carbons, ChemSusChem 8 (11) (2015) 1867–1874.
[41] A.Y. Mottlau, N.E. Fisher, Measurement of pore volume by a titration technique, Analytical Chemistry 34 (6) (1962) 714–715.
[42] M. Aslan, et al., Polyvinylpyrrolidone as binder for castable supercapacitor electrodes with high electrochemical performance in organic electrolytes, Journal of Power Sources 266 (1) (2014) 374–383.
[43] Q. Abbas, et al., Effect of binder on the performance of carbon/carbon symmetric capacitors in salt aqueous electrolyte, Electrochimica Acta 140 (2014) 132–138.
[44] H. Gerischer, The Impact of Semiconductors on the Concepts of Electrochemistry, Electrochimica Acta 35 (11–12) (1990) 1677–1699.
[45] A.A. Kornyshev, N.B. Luque, W. Schmickler, Differential capacitance of ionic liquid interface with graphite: the story of two double layers, Journal of Solid State Electrochemistry 18 (5) (2013) 1345–1349.
[46] C. Schütter, et al., Activated Carbon, Carbon Blacks and Graphene Based Nanoplatelets as Active Materials for Electrochemical Double Layer Capacitors: A Comparative Study, Journal of the Electrochemical Society 162 (1) (2015) A44–A51.
[47] H.A. Andreas, Self-discharge in electrochemical capacitors: A perspective article, Journal of the Electrochemical Society 162 (5) (2015) A5047–A5053.
[48] C.R. Pérez, et al., Structure and electrochemical performance of carbide-derived carbon nanopowders, Advanced Functional Materials 23 (8) (2013) 1081–1089.
[49] J.K. McDonough, et al., Influence of the structure of carbon onions on their electrochemical performance in supercapacitor electrodes, Carbon 50 (9) (2012) 3298–3309.
[50] P. Krtil, L. Kavan, P. Novak, Oxidation of Acetonitrile-Based Electrolyte Solutions at High Potentials, Journal of The Electrochemical Society 140 (12) (1993) 3390.
[51] P. Kurzweil, M. Chwistek, Electrochemical stability of organic electrolytes in supercapacitors: Spectroscopy and gas analysis of decomposition products, Journal of Power Sources 176 (2) (2008) 555–567.
[52] D. Cericola, et al., Effect of Water on the Aging of Activated Carbon Based Electrochemical Double Layer Capacitors During Constant Voltage Load Tests, International Journal of Electrochemical Science 6 (4) (2011) 988–996.